Molecular springs, muscles, rheostats, and precessing gyroscopes: from review to preview†

Michael J. Marsella,* Shohreh Rahbarnia and Nathan Wilmot

Received 25th September 2006, Accepted 20th November 2006
First published as an Advance Article on the web 9th January 2007
DOI: 10.1039/b613891h

The concepts of molecular springs and gyroscopes have existed for some time, and there have been numerous reports published about these fascinating topics. Here we describe our interest in this topic, reviewing our initial progress. This is not a complete story, rather an offering of synthetic strategies, interesting molecular structures, observations, and possibilities. In many cases, the "properties" component of the structure–property relationship for a given compound is the result of a computational prediction. Given the present state of theoretical chemistry, a computer's predictive power can far exceed that which can be presently accomplished by existing experimental analytical means. The theoretical results reported here allude to intriguing possibilities. Hopefully, this intrigue will help catalyze the development of definitive, albeit rather esoteric, single-molecule analytical experiments. The intentionally speculative nature of this review is intended to stimulate new challenges for and perspectives from those in related fields of interest; hopefully presenting a preview of what is to come.

Department of Chemistry, University of California, Riverside, Riverside, CA 92521, USA

† Electronic supplementary information (ESI) available: Animation of a dynamics calculation on a helical pentaaryl, animation of the pitch range of a single thiophene-fused [8]annulene and a movie file showing the early stages of conversion to rotation and precession for compound **PG-1**. See DOI: 10.1039/b613891h

Molecular springs

A macroscale spring is a device typically composed of a coiled material, capable of being stretched (tension springs) or compressed (compression springs). For metal springs, a simple atomistic description states that atomic interactions are displaced from

Professor Michael Marsella received his BS in Secondary Education (Minor in Chemistry) from the University of Rhode Island in 1990. He went on to receive his PhD in Chemistry from the University of Pennsylvania under the direction of Professor Timothy M. Swager (now at MIT). After two years as a NIH Postdoctoral Scholar at Caltech with Professor Robert Grubbs, he began as an Assistant Professor of Chemisty at University of California, Riverside. He was promoted to Associate Professor in 2003. His research laboratory focuses on the design and synthesis of conjugated materials and single-molecule devices.

Shohreh Rahbarnia received her BS in Chemistry from the University of California, Irvine in 1997. She went on to receive her MS from California State University, Sacramento under the direction of Dr Cynthia Kellen-Yuen. She is currently a PhD candidate in Chemistry at the University of California, Riverside under the direction of Professor Michael J. Marsella.

Nathan Wilmot received his BS in Chemistry (Minor in Physics) from Kutztown University in 2002. In 2006, he received his PhD from the University of California, Riverside under the direction of Professor Michael J. Marsella. Following graduation, he accepted his current position of Senior Chemist at The Dow Chemical Company in Freeport, TX in the Polyurethanes R&D department.

Michael J. Marsella

Shohreh Rahbarnia

Nathan Wilmot

an equilibrium state when a force is applied, thus accessing a higher-energy state. A spring's restoring force is the return to the equilibrium state of atomic structure and bonding. This is true of both coiled and non-coiled springs, such as leaf springs and spiral springs.

Given the above description, one could define almost any conformationally flexible molecule as a spring. For example, consider a force applied to a molecule such that bond lengths, bond angles, and/or dihedral angles are perturbed from equilibrium, thus raising the energy of the molecule. Once the force is released, the molecule will return to its equilibrium conformation (that is, assuming a transition state between conformers is not reached in the process). Although most molecules can fit this definition to some extent, fewer satisfy the requirements of maximizing extension (or compression) within a deep-well global minimum. For example, conversion of a hydrocarbon from an all s-*trans* to all s-*cis* conformation would be analogous to compression. However, the energy barriers that lead to other conformers are easily overcome, thereby negating the concept of a restoring force. In other terms, the path between s-*trans* and s-*cis* does not exist in a sufficiently deep energy well on the potential energy surface to avoid diversion to other conformations. Fig. 1 reports the analogy between spring function and bond rotation, using bithiophene as the example molecule. Oligothiophenes will serve as the basis of our molecular spring.

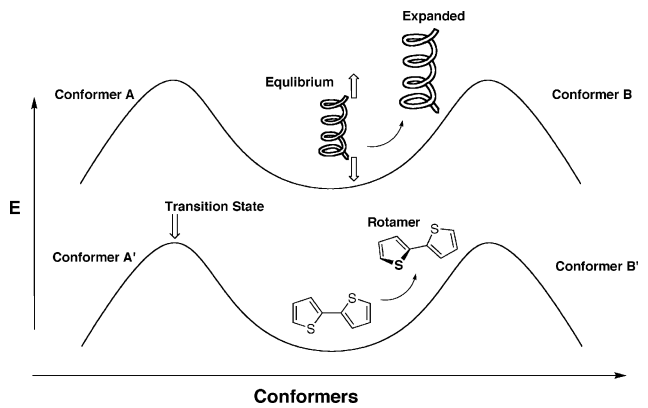

Fig. 1 Showing the reversible behavior of macroscopic springs and molecules (bithiophene), as they are physically displaced from equilibrium geometry. As long as the displacement corresponds to energy less than the transition state boundaries, the perturbation will be reversible.

Helicenes[1–9] are one class of molecules capable of functioning as molecular springs. Their rigid helical backbone does not allow for multiple conformations, and the equilibrium conformer lies in a sufficiently deep energy well to allow restoration after compression and extension. The dynamic behavior of helicenes, specifically for application as actuator materials,[10–12] is currently being investigated by the King group at the University of Nevada, Reno.[13] By definition, helicenes are conjugated, and it is no coincidence that they are highlighted here as an example. For reasons that will be introduced later in this article, compositional requirements for our molecular spring include both a helical *and* conjugated backbone, and our preference is a motif other than a traditional helicene.

Our building block of choice is the aromatic heterocycle, thiophene (Fig. 2). Poly- and oligothiophenes have served as major workhorses in organic materials applications, serving the spectrum of electronic properties from semiconductors to "synthetic" metals.[14–17] In addition to the "tunable" electronic properties of oligomers and polymers, the thiophene ring itself has two synthetic attributes that are highly desirable for our purposes. First, the thiophene ring has two pairs of reactive sites for carbon–carbon bond formation, with each pair having unique chemical reactivity. In general, the 2- and 5-positions (α-positions) are more reactive than the 3- and 4-positions (β-positions) with respect to electrophilic aromatic substitution, Grignard formation of the corresponding halothiophenes, thienyl lithium formation, and cross-coupling reactivity. Second, thiophyne is rarely observed under conditions that would otherwise convert *o*-substituted benzene to benzyne. The selective bromination at α-positions, and lithium–halogen exchange occurring exclusively at the 2-position of 2,3-dibromothiophene (without thiophyne formation[18]) are key transformations in many of our synthetic strategies.[10,19–25]

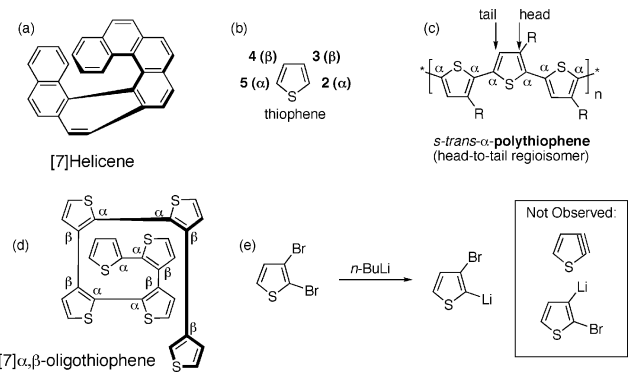

Fig. 2 Showing (a) a prototypical helicene composed of seven fused [6]annulenes; (b) the aromatic heterocycle, thiophene; (c) repeat unit of s-*trans*-α-polythiophene; (d) a helical α,β-oligothiophene composed of seven rings; and (e) illustrating the selectivity and reactivity of 2,3-dibromothiophene: treatment with BuLi results exclusively in the 2-lithio species. Thiophyne and the 3-lithio species are not observed.

How does one make a helical oligothiophene? First, let us consider the more traditional, linear polythiophenes. Seminal work by McCullough and co-workers has taught that head-to-tail regiochemically pure polythiophenes that are **all-α-fused**, **all *s-trans***, and **co-planar** offer the highest conductivities of all β-alkyl-substituted α-polythiophenes.[26–28] Key terms were bolded for emphasis. While it is conceivable to envision the same α-fused polymer to exist in a helical conformation (*i.e.*, all s-*cis*), Merck Molecular Force Field (MMFF) calculations report an energetic penalty for each bithiophene unit converted from s-*trans* to s-*cis.* Specifically, a conformer search of a 13-mer oligothiophene establishes the planar (all s-*trans*) conformer as the global minimum, with the helical (all s-*cis*) conformer lying *ca.* 13 kcal mol^{-1} higher in energy (Fig. 3). Between these extremes exist other possible combinations of s-*cis* and s-*trans* conformers. Thus, α-oligothiophenes are significant for their preference to be co-planar; a scenario optimal for high conductivity, but not helicity. As both the physical length and effective conjugation length of an unsubstituted, s-*trans* α-oligthiophene increases, both the band gap ($E_g = E_{LUMO} - E_{HOMO}$) and solubility decrease. Thus, electronic

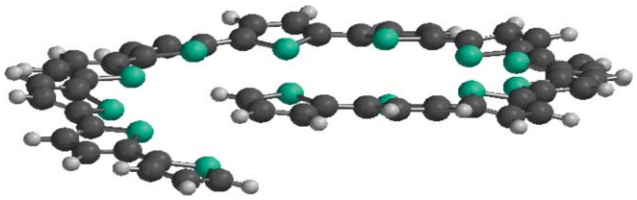

Fig. 3 One helical turn of a 13-mer α-oligothiophene (s-*cis*) is predicted by MMFF to be 13 kcal mol^{-1} higher in energy than the linear conformer of the same system (s-*trans*).

conductivity can be conveniently tuned by length and degree of co-planarity, but solubility issues must also be addressed, typically by addition of alkyl side-chains.

In contrast to all-α-fused oligothiophenes, our efforts have focused on α,β-oligothiophenes (*ortho*-oligothiophenes).[23–25] The sterics associated with this regioisomer preclude the co-planarity of adjacent thiophene rings. Subjecting α,β-tetrathiophene regioisomers to the same MMFF conformer search process described above yields opposite results: the global minimum of each regioisomer is a compact helix. Higher in energy (*ca.* 0.8–2.2 kcal mol^{-1}) exists an extended helical conformer. These results are summarized in Fig. 4. Another report from our laboratory claimed α,β-oligothiophenes to be "reliable helical scaffolds."[23]

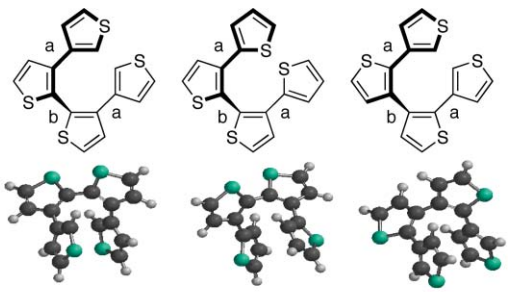

compact helix			
dihedral a:	46.6°	41.6°	41.2°
dihedral b:	58.6°	59.9°	58.1°
extended helix			
ΔE (kcal/mol):	1.9	2.2	0.8
dihedral a:	43.0°	41.2°	36.5°
dihedral b:	115.8°	110.6°	119.1°

Fig. 4 Showing three α,β-tetrathiophene oligomers, and reporting dihedral angles for both the global minimum structure (compact helix; also shown as ball-and-stick structure), and higher energy extended helix conformer. The energy difference between compact and extended helix is also given. All values were determined from MMFF conformer searches.

The synthesis of α,β-oligothiophenes is facilitated by unique reactivity of the α- and β-thienyl positions (as described above). Scheme 1 reports three different synthetic routes that we have used to prepare helical oligomers. Note that the synthesis accommodates either thiophenes or phenyl rings at each terminus (thus, the term "oligoaryl" should technically be used). In general, biaryls and teraryls are prepared by nickel catalyzed cross-coupling chemistry,[29] and halogenation is used to direct lithiation (*via* lithium–halogen exchange). The resultant organolithium species can be converted to an organostannane for tandem cross-coupling (Scheme 1a), used as the nucleophile for a double addition–elimination with octafluorocyclopentene (Scheme 1b),[30–32] or oxidatively coupled using Fe(III) (Scheme 1c).[33]

In addition to an overview of our synthetic methods and oligomer composition, Scheme 1 also reports the structures determined using single crystal X-ray analysis. In all cases, the compact helical conformation observed in the single crystal X-ray structural analysis was predicted by MMFF calculation of the equilibrium conformer. The inset in Scheme 1a shows an overlay of three structures: the experimentally determined single crystal X-ray analysis structure, and two calculated global minimum conformers (MMFF and BLYP/6–31G(d)). The similarity found between experimentally determined and predicted structure is excellent.

The MMFF calculated energy well associated with each S–C–C–S dihedral angle between adjacent thiophene rings was found to be the most dominant force biasing the compact helical conformation.[23] The barriers to this energy well can be visualized by molecular dynamics calculations. Fig. 5 shows the superimposition of four frames of a molecular dynamics simulation of a helical pentaaryl (individual frames colored as blue, green, yellow, black). The selected frames illustrate that motion about the torsional angle associated with the two thiophene rings labeled as A and B in Fig. 5. The "unspectacular" range of motion portrayed in Fig. 5 is what is most significant, as it illustrates that adjacent rings approach, but reverse direction prior to eclipsing or passing one another (this dynamics calculation is available as a movie file in the ESI†). Not surprisingly, the motion is reminiscent of a vibrating spring.

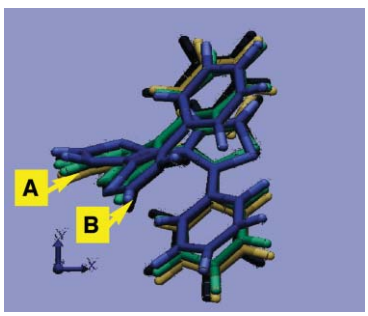

Fig. 5 Showing four frames of a dynamics calculation on a helical pentaaryl. Rings labeled A and B approach, but do not eclipse or pass one another, thus maintaining the helical conformation. Animation of this dynamics calculation is available as a movie in the ESI.†

Molecular muscles

Our interest in helical oligomers originated from possible application in the emerging field of *bio-inspired nanotechnology.* Using more traditional terms, we are interested in integrating physical organic and polymer chemistry to prepare macromolecules with dynamic properties that may be attenuated by external forces. Namely, we are interested in preparing "molecular muscles" that are capable of expansion and contraction under an electrical bias.[10–12,22,25,34,54] Our first effort in this area focused on a polymer of thiophene-fused [8]annulene repeat units. Each unit of the polymer is defined as an "actuator synthon," capable of lengthening and contracting as a function of redox state. The polymer can be envisioned as mechanically mimicking a bellows, whereby each [8]annulene monomer is one convolution of the bellows, and the pitch of each convolution changes as a function of oxidation state (see Fig. 6). This earlier work is reviewed elsewhere, and will not be further discussed here (an animation of the pitch range of a

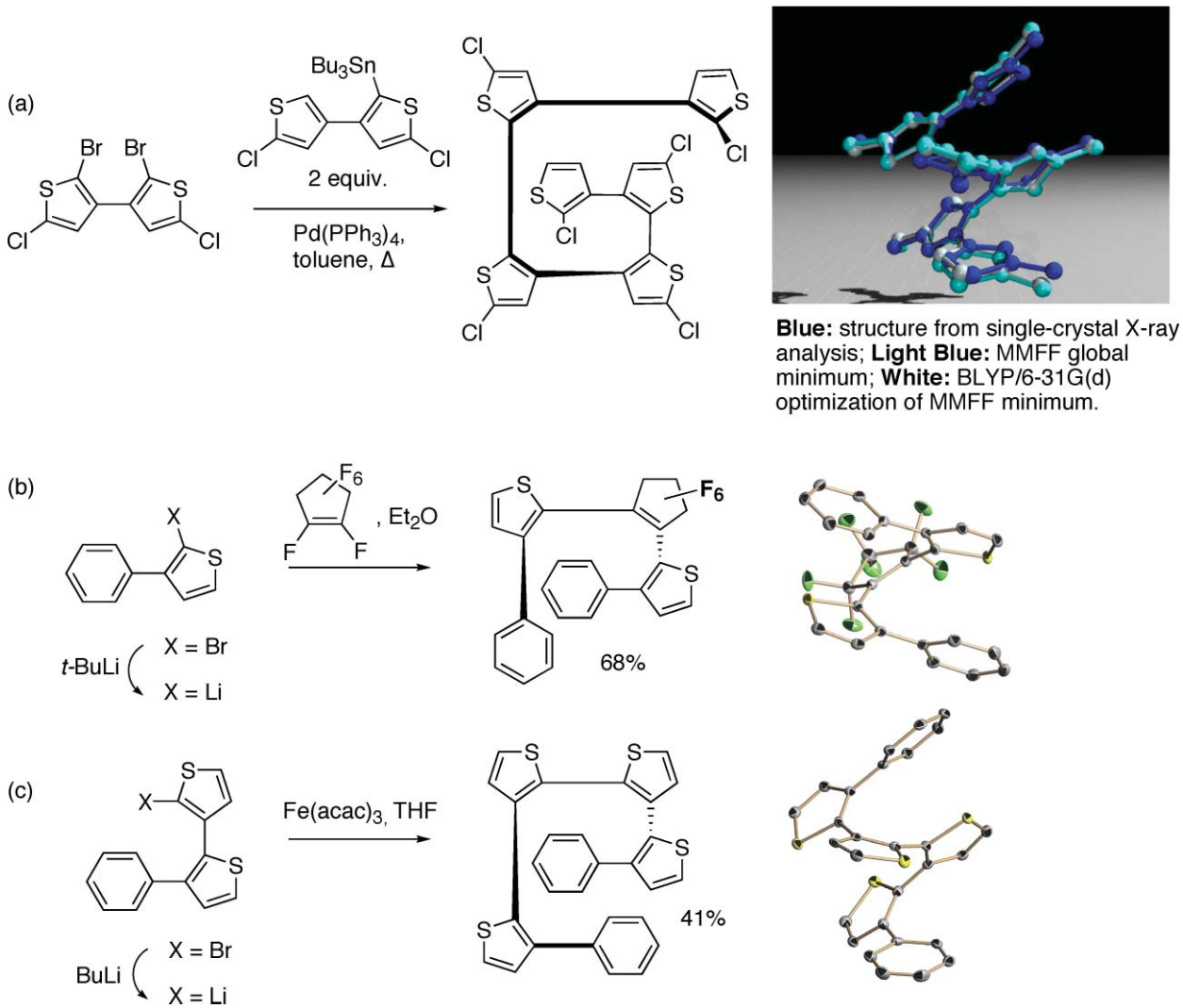

Scheme 1

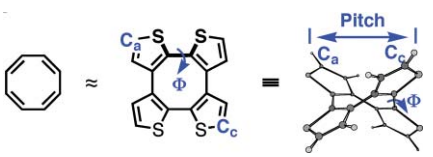

Fig. 6 The thiophene-fused [8]annulene (tetra[2,3-thienylene]) is envisioned as one convolution of a bellows. For the corresponding polymer, a change in pitch for each convolution is induced by a change in redox state, yielding an additive expansion or contraction process (*i.e.*, bellows-like expansion and contraction). An animation of the pitch change for a single convolution is provided as a movie file in the ESI.†

single thiophene-fused [8]annulene is provided as a movie file in the ESI†).

To compliment our bellows-concept, an actuator based on a spring seemed to us a valid proposal.[13] Ideally, there would be a conjugated helix (our molecular spring, above), with the possibility for p-orbital interactions not only in a side-on sense between adjacent rings, but also in a head-on sense between adjacent turns of the helix. Calculations predicted that upon oxidation or reduction, such a helix would contract from its equilibrium neutral conformer length. We propose that the contraction process is driven by increased orbital interaction, thus best delocalizing the charge. Fig. 7 illustrates this concept, showing (a) neutral redox state: non-ideal overlap of adjacent orbitals (red; representing orbital interaction between adjacent rings) and minimal head-to-head orbital interactions (red–blue), and (b) charged redox

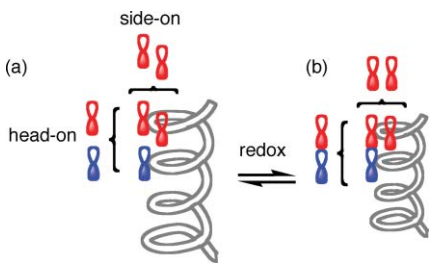

Fig. 7 Showing (a) equilibrium conformer of a conjugated helix, and (b) contracted form of the same helix, as a result of oxidation or reduction. The red–red orbital interaction represents side-on overlap, and the red–blue orbital interaction represents head-to-head overlap. Contraction (form b) is believed to increase both types of overlap.

state: improved side-on and head-to-head orbital interactions (both red–red and red–blue, respectively). Here, note that the length of the helix is a function of the dihedral angles between adjacent rings. Thus, side-on orbital interactions increase as dihedral angles decrease. Commensurately, a decrease in dihedral angles shortens the helix, thereby increasing head-on orbital interactions.

To test this theory, we geometry optimized both compounds **Hex-1** and **Hex-1**$^{2+}$ (HF 6–31G(d)). Fig. 8 shows the three unique bonds (labeled *a*, *b*, and *c*) associated with the three unique dihedral angles for the given helical hexamer. In the neutral form, the calculated bond lengths range from (*a*) 1.475 Å, (*b*) 1.48 Å, and (*c*) 1.476 Å. The corresponding dihedral angles are (*a*) 63.6° and (*b* = *c*) *ca.* 46°.

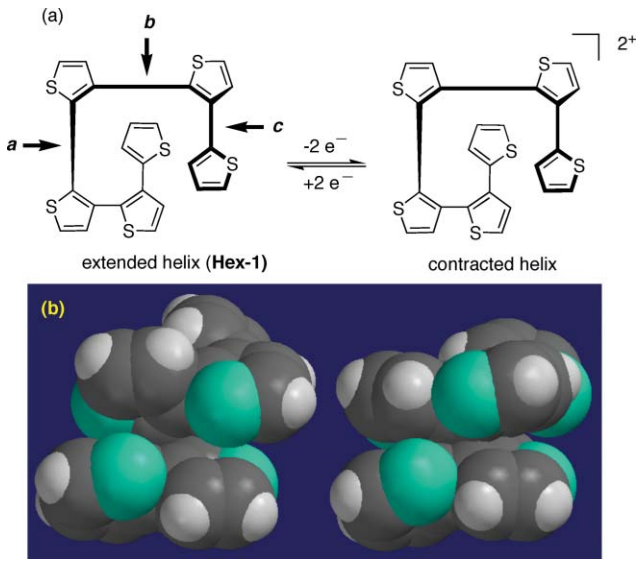

Fig. 8 (a) Defining the bonds in **Hex-1** (see corresponding text). (b) Space filling models of **Hex-1** (left) and **Hex-1**$^{2+}$ (right, contracted form).

The equilibrium geometry of **Hex-1**$^{2+}$ reports the desired contraction. Bond *a* develops considerable double bond character, with its length decreasing from 1.775 Å to 1.339 Å. The corresponding dihedral angle reduces from 63.6° to 5.3°. The dihedral angles associated with bonds *b* and *c* also decrease in value from 46° to 37.5°. Summing the NBO[35–40] atomic charges for each ring reveals that *ca.* 50% of the 2^{+} charge is localized onto the central bithiophene unit. The closest carbon–carbon atomic contacts in **Hex-1**$^{2+}$, reflecting the head-to-head orbital interaction discussed above, is 3.42 Å. In the neutral form, this same distance is 3.64 Å. In accord with prediction, contraction and oxidation are commensurate, and reinforce the applicability of helical oligoarenes to function as molecular muscles. This contraction can be viewed in Fig. 8b, which shows space-filling models of **Hex-1** and **Hex-1**$^{2+}$.

What else can be speculated from calculation? The following concepts, entitled "Molecular Rheostats" and "Molecular Precessing Gyroscopes," have foundation in theory, and are supported by initial calculations. However, any discussion of these applications mandates assumptions to be made. Others have established relevant experimental groundwork. However, for our purposes, what exists are puzzle pieces yet to be connected. The missing puzzle pieces are esoteric single-molecule experiments likely to be commonplace in the near future, but not at present. Regardless, design and synthesis can continue, with theory serving (at least temporarily) as the surrogate experimental proof. We thank the editors and reviewers for allowing not only the standard review of our published work, but also a *preview* of potential applications (muscles, rheostats, and rotors). Our speculation is intentional, and is offered to further stimulate discussion about the future of molecular machines, devices, and related phenomena.

Molecular rheostats

A rheostat can be defined as a variable resistor that is attenuated by a mechanical process. In our design, the macroscopic process of "turning a knob" to attenuate resistance (and hence current), is mimicked at the molecular level by stretching a conjugated helix. Specifically, we investigate the possibility of integrating scanning tunneling microscopy (STM) experiments with helical oligomers, as a route into force-attenuated conductivity (*i.e.*, a molecular rheostat).

The requisite experiment is based on STM experiments recently reported to yield *reproducible measurements of single-molecule conductivity.*[41] In this remarkable work, Venkataraman and Nuckolls showed that single molecule conductivity of terminal aliphatic and aromatic diamines could be reproducibly measured *via* STM. By adsorbing one amine terminus onto a gold surface and the other onto the STM tip, conductance was measured as a function of tip–surface distance until either end was desorbed. The choice of amino functionality in the experiments was vital due to the single coordination geometry that exists between amine nitrogens and a gold surface. Amines only add to unsaturated gold sites, the so-called "adatoms," *via* donation of the nitrogen lone-pair to a vacant Au orbital, in a well defined geometry. More commonly employed functional groups, such as thiols, add in multiple geometries. This, combined with the consideration that amines are not subject to oxidative oligomerizations, leads to consistent conductivity curves for a given substrate over many cycles. It was found that clear conductance data could be obtained for aliphatic substrates as large as 1,8-octanediamine, and that a minimal steric bulk about the nitrogen led to the most well defined conductance. For our purposes, we emphasize that accurate measurements of single-molecule conductivity may be obtained *via* STM, simultaneous with physical "pulling" on the molecule of interest. The assumption is that the STM tip may serve both as the mechanical element of the rheostat, as well as the probe to accurately measure changes in conductance through the extending helix.

Our design of a molecular rheostat requires the following four ideal characteristics:

Helical oligomers ("molecular springs") must demonstrate an effective conjugation length that varies as a function of molecular conformation.

(1) Any changes in conjugation must translate to changes in molecular conductance.

(2) The termini of the helix must be functionalized to allow adsorption between metal surface and STM tip adatoms.

(3) Using the STM tip to generate mechanical force, the helix must stretch from a compact helical conformation (dihedral angles <90°) to an extended helical conformation (>90°).

To simplify calculations of the molecular rheostat, we first reduced the composition of the helical oligomer to a helical s-*cis*-*z*-polyene (1,3,5,7,9-decapentene). The length of this helix is a direct function of the dihedral angles between adjacent –HC=CH– moieties of the backbone. In an ideal case, the fully extended system, registering 180° dihedral angles throughout, would experience complete overlap of the pi-system, establishing a conjugation maximum.

With one end of the helix fixed in space, a unidirectional external force could be applied such that the helix is pulled from its compact coil conformation to its fully extended state. Commensurately, conjugation would decrease to a minimum as dihedral angles approach 90°. Further extension would again increase conjugation (dihedral angles >90°). Overall, orbital overlap (effective conjugation length) should respond non-linearly as a function of lengthening from a compact coil to a fully extended state.

We employed outer valence green function (OVGF) calculations to gain ionization potentials (I_p) and electron affinities (E_a), and used these differences in energy as a qualitative predictor of single molecule conductivity. The assumption is that extent of orbital overlap attenuates effective conjugation length, which in turn affects electron/hole mobility, μ. Conductivity and mobility are related by eqn (1).

$$\sigma = ne\mu \quad (1)$$

where σ = conductivity, n is the number, e the type of carrier, and μ is carrier mobility. This assumption served the basis for ionoresistive conjugated polymers of the type previously reported by Swager and Marsella.[42,43] In both cases, induced conformational changes are anticipated to be the cause of changes in conductivity. In this present work, we calculate the energies of I_p (*i.e.*, HOMO) and E_a (*i.e.*, LUMO), and use this difference as a probe of effective conjugation; the smaller the difference, the greater the effective conjugation, the greater is the potential for increased carrier mobility, and the higher the molecular conductivity.

A HF/6–31G(d) OVGF analysis of a C2-symmetric helical decapentaene was performed, whereby C=C–C=C dihedral angles were constrained to values of 30°, 60°, 90°, 120°, 150°, and 180° (corresponding to an extension from compact coil to linear conformer; see Fig. 9). By definition, these values also report the angle between atomic p-orbitals on adjacent ethylene moieties of the polyene. A first-approximation mandates that there are no long-range orbital interactions at the 90° conformer, as all ethylene moieties are oriented such that adjacent p-orbitals are orthogonal and non-interacting.

The I_p and E_a determined from OVGF calculations are plotted in Fig. 1, as change in I_p and E_a relative to the 30° starting point. Note the plot is *relative* to the 30° dihedral angle conformer, *versus* dihedral angle, and should not be misinterpreted as a crossing of I_p and E_a at *ca.* 150°. The values posted adjacent to data points report the pole strength, which is a measure of probability of each corresponding excitation (maximum value of pole strength is 1.0). Thus, there are four parameters for each dihedral: ionization potential, electron affinity and the two corresponding values of pole strength. The most striking trend in the OVGF data is the non-linear change of both I_p and E_a, with inflection points occurring at the 90° dihedral conformation. This trend matches the predictions made above. Given that π-orbital overlap, I_p, and E_a should qualitatively reflect conductance, it follows that a uniaxial force that extends the molecular helix should be capable of attenuating single-molecule conductance, thus establishing a molecular rheostat. More detailed computations are currently underway, as are the syntheses of helical oligomers specifically designed to meet the above criteria and goals.

Precessing molecular gyroscopes

Herein we have made several allusions to macroscopic objects being reproduced at the molecular level. This is illustrated in our previous discussions of molecular springs and rheostats. A more

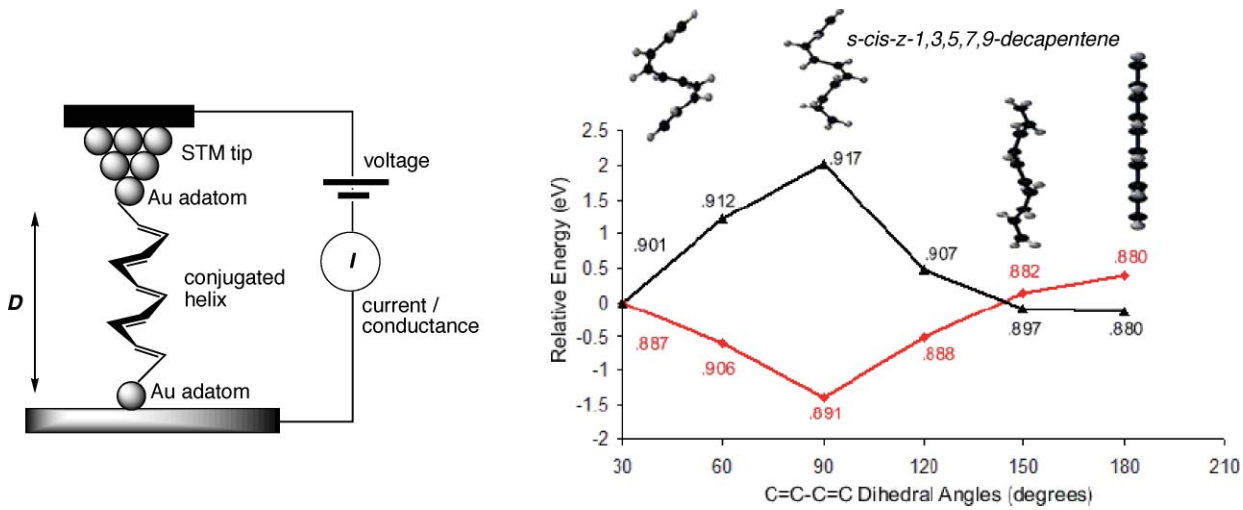

Fig. 9 Conceptually illustrating the molecular rheostat: adatom adsorption of a conjugated helix serves as the variable resistor, which is attenuated by unidirectional pulling by the STM tip (left). In turn, orbital overlap varies from 30° to 180°, reaching a minimum of overlap at the 90° angle (orthogonal orbitals), and a maximum of overlap at 180°. The graph on the right reports energies of ionization potential (red; HOMO) and electron affinity (black; LUMO), relative to the 30° dihedral angle starting point. Pole strengths are also reported adjacent to data points (see text). In theory, molecular conductivity is measured by the STM, and correlates with the HOMO–LUMO gap determined from the data plot.

general question regarding this concept is, can macroscopic and molecular machines share intrinsic property characteristics? Or does the interface of classical mechanics and quantum mechanics complicate (or doom) the translation? Kelly has published a spectacular paper on this topic, targeting the concept of a molecular ratchet, illustrating clearly the disconnection that may occur during the molecularization of a macroscopic device.[44–46] In this final section, we hypothesize on the molecularization of a precessing gyroscope.

By definition, and as shown in Fig. 10, a precessing gyroscope contains two orthogonal axes of rotation. Precession about the *y*-axis results from rotation about the *x*-axis. The Newtonian forces that dictate rate of precession include the vector product of the angular momentum of the rotor (L), which is a result of the rotor's moment of inertia ($I = 0.5\ mr^2$) and angular velocity (ω), and the torque ($\tau = mgr'$). The precession rate (Ω) is estimated by eqn (2):

$$\Omega \approx mgr'/I\omega \qquad (2)$$

Before further discussion of *precessing* molecular rotors, we note that Michl has compiled an excellent review of molecular rotors and motors,[47] summarizing the contributions of his own group, and those of Moore,[48] Garcia-Garibay,[49] Tour,[50] Gladysz,[51] and many others. Other critical work to be mentioned includes Gimzewski's visualization of a single-molecule rotor on a Cu(100) surface[52] and Feringa's light-driven rotor anchored to a gold nanoparticle surface.[53] The collective precedent for our exploration includes the properties of the molecular rotors described in this review, as well as the potential to monitor rotary motion on a surface.

Relating eqn (2) to a molecule adsorbed to a surface mandates that the term, "g" be (re)defined by intramolecular and molecule–surface attractive forces, since the universal constant of gravitation (6.7×10^{-11} N m^2 kg^{-2}) is not relevant. All other terms of the equation will be presumed applicable. The questions we pursue are, will rotation and precession be correlated at the molecular level (as it is in the macroscopic world)? If yes, does it vary as a function of intramolecular and surface attractive forces? The first part of this two-part question is answered by the intrinsic properties of certain molecules, as can be shown in the case of 2,5-heptadiyne.

The frequencies for 2,5-heptadiyne (HF/3–21G(d)) were calculated, and displacement vectors are shown in Fig. 11. If one methyl group of 2,5-heptadiyne is presumed to be fixed in space, the resulting system becomes analogous to the precessing gyroscope motif, in the sense that one methyl group is the base, one is the rotor, and they are connected by two (nearly) orthogonal axes of rotation. Using this frame of reference, we may re-define the three lowest energy vibrations as the following processes (from highest

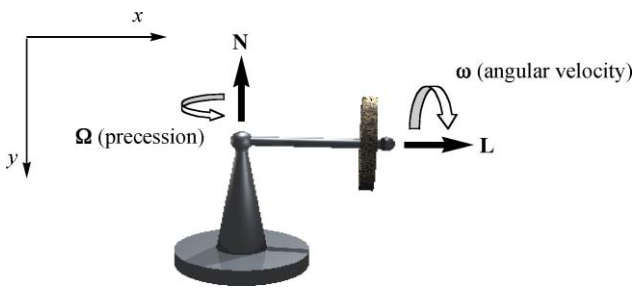

Fig. 10 Depicting a precessing gyroscope. Two orthogonal axes of rotation are attached to a fixed base (black) and rotor (marble). Precession about the *y*-axis results from rotation about the *x*-axis.

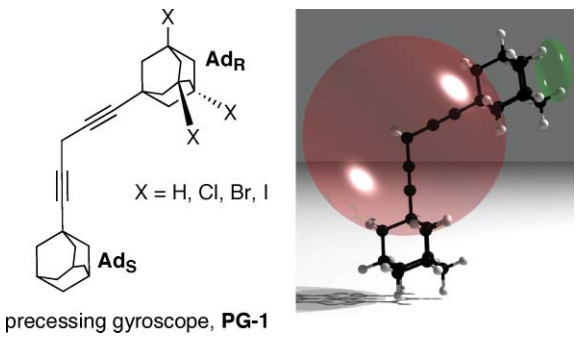

Fig. 12 Showing hypothetical precessing gyroscope, **PG-1**. The inset illustrates the VDW cut-off volume (red sphere) used in the molecular dynamics calculations. The green sphere locates the region of halogen functionalization. Note halogens are outside of the VDW cut-off.

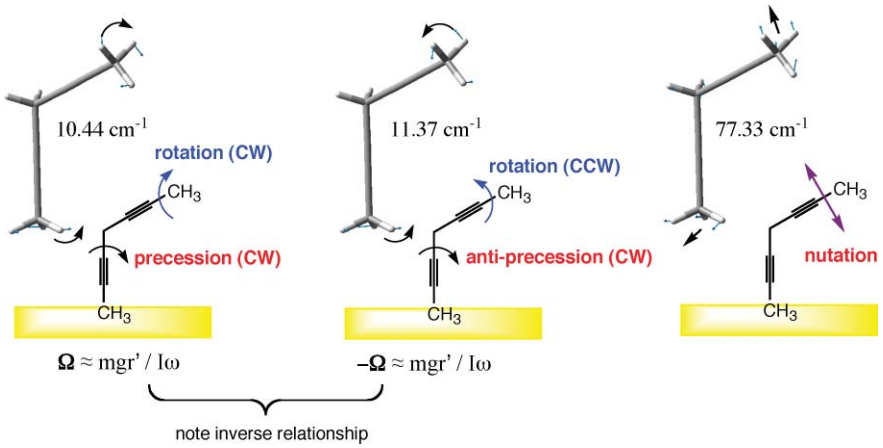

Fig. 11 Showing the as-calculated frequency displacement vectors for 2,5-heptadiyne, and illustrating how, when fixed to a surface, they translate to be analogous to the processes associated with precessing gyroscopes.

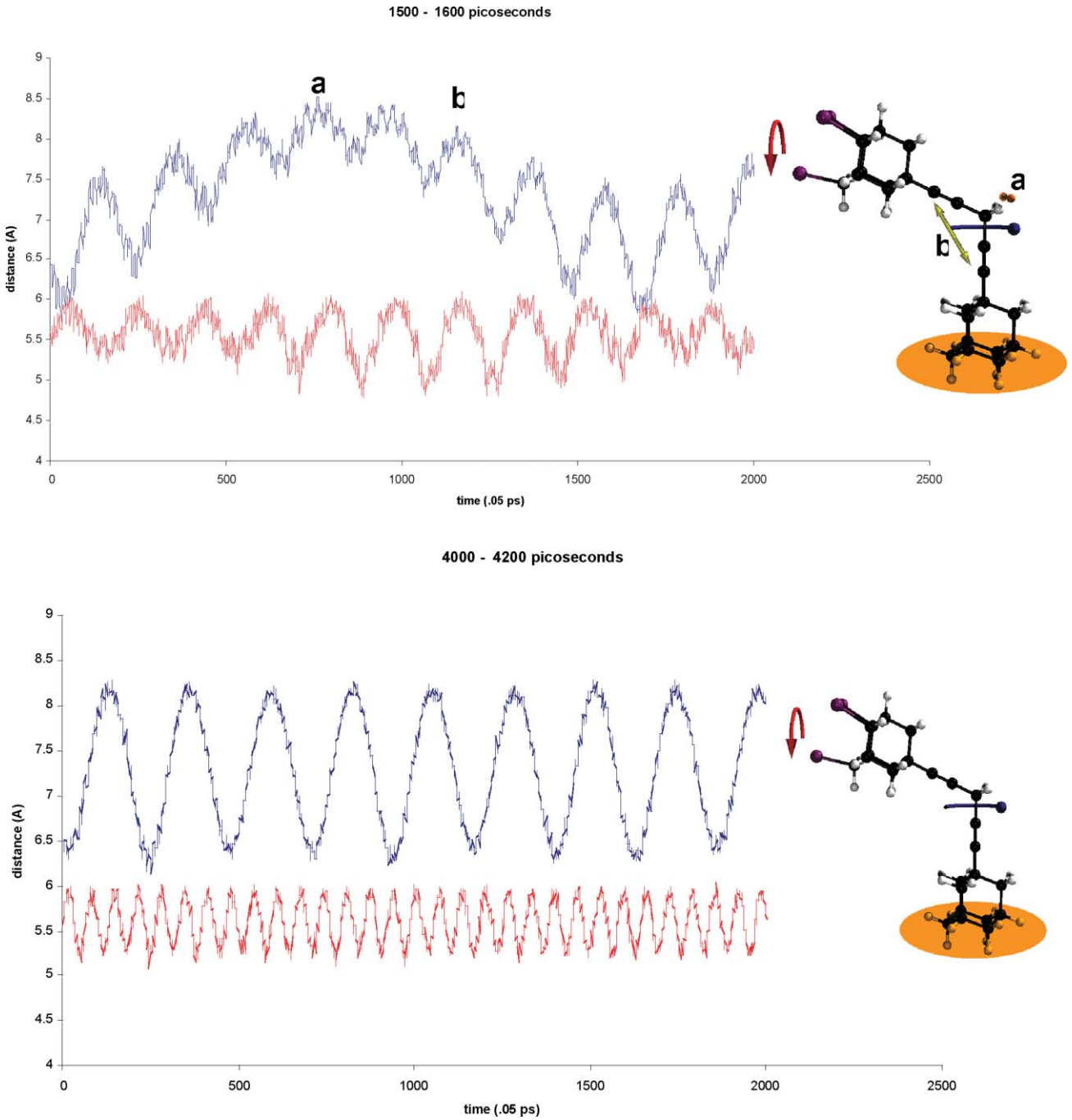

Fig. 13 Evolution of precessing gyroscopic motion in **PG-1** (Ad_R–Br_3): (**TOP**) early in dynamics run where (a) describes waggle about methylene group and is a minor periodic function, (b) represents nutation of gyroscope (indicated by yellow double-headed arrow), blue major wave is precession (blue curved arrow), and red waves represent rotation (red curved arrow). (**BOTTOM**) after 4 nanoseconds, an equilibrium state is reached; *nutation and waggle have been almost completely translated into precession (blue) and rotation (red)*.

to lowest energy): (i) nutation (77.33 cm^{-1}), (ii) rotation/anti-precession (11.37 cm^{-1}), and (iii) rotation/precession (10.44 cm^{-1}, see Fig. 11). Thus, the lowest frequency mode corresponds to that motion analogous to a macroscopic precessing gyroscope (*i.e.*, eqn (1)). Under ideal conditions, 2,5-heptadiyne may function as a precessing gyroscope. Throughout the remainder of this discussion, "ideal" implies that rotor–solvent effects are ignored.

Our second study subjected the bisadamantyl precessing gyroscope (hypothetical) compound **PG-1**, to a dynamics calculation. To mimic a surface, we defined one adamantyl unit as stationary (Ad_S), and the other as a rotor (Ad_R). To Ad_R was attached three halogens (Ad_R–Cl_3, Ad_R–Br_3, and Ad_R–I_3), resulting in three new compounds, each differing in rotor mass. By limiting van der Waals (VDW) interactions in the dynamics simulations to 7 Å,

these halogens do not interact with Ad_S. Fig. 12 illustrates that the allowed VDW interactions are roughly limited to the atoms enclosed within the red balloon. The green balloon represents sites for halogen substitution.

To emphasize, the halogen substitution will perturb the rotor mass term, and thus the moment of inertia, but not the attractive force term, *g*. For each of the three unique molecular dynamics reactions, the correlated rates of rotation and precession varied according to mass, but the term "*g*" was found to be nearly constant ($1.98 \pm 0.06 \times 10^{20}$ m/s^2 mol).

Lastly, and perhaps most visually impacting, is the obvious evolution of correlated precession and rotation, as determined by molecular dynamics. This is reported in Fig. 13; showing molecular dynamics data related to compound **PG-1** (Ad_R–Br_3). As described in the caption of Fig. 13, early molecular dynamics events of compound **PG-1** include waggle, nutation, rotation, and precession. Upon equilibrium, waggle and nutation (higher energy vibrational modes; see Fig. 12) convert to pure rotation and precession, and eqn (2) *is obeyed.* A movie file showing the early stages of conversion to rotation and precession is provided in the ESI.†

In practice, achieving a system that obeys the properties of a classical precessing gyroscope should be possible by thermally biasing high populations of the lowest vibrational mode. Given that rotor mass, rotation, and precession are related, it is feasible to engineer a macromolecule with a rotor massive enough to promote precession in the Hertz frequency range (and, ideally, without interference from surface phonons).

It is worth noting that although coupled rotation–precession is governed by eqn (2), the phenomenon of molecular gearing[54] is not as rigorously quantified, in the sense that slippage can take place at random intervals. In other terms, the pure rotation–precession mechanism is not prone to slippage (*i.e.*, mistakes), as is the process of gearing. Furthermore, the relative rates of rotation within a precessing gyroscope and a geared system are not governed by the same laws of physics (*i.e.*, eqn (2) *versus* gearing ratios), thus creating unique rotational profiles for each class of rotor. We emphasize that the ethynyl "axles" employed ensure that all rotating bodies are beyond intramolecular VDW radii, ensuring that gearing is *not* taking place.

In summary, to the field of molecular devices we have supplemented the concepts of molecular springs, molecular rheostats, and gyroscopes. Beyond the concrete discussion of synthesis, computational chemistry has provided predictions of physical properties. In the ideal "silicon world" of computational chemistry, the concepts are sound and the possibilities are intriguing. Now, this exercise in the sublime must bear the burden of experimental proof. The speculative nature of this review (preview?) was entirely intentional (*i.e.*, aspiring to works similar to Hopfield's proposal of a "shift register memory,"[55]), and hopefully adding productively to the list of challenges on queue for future studies.

Acknowledgements

The compiled research has been funded, in part, by the National Science Foundation, Research Corporation, Petroleum Research Fund, DuPont, and UC Riverside. SR and NW are recipients of the Department of Education GAANN fellowship. We thank Dr Benjamin King (University of Nevada, Reno) for assistance with molecular dynamics calculations.

References

1 H. Wynberg, M. B. Groen and H. Schadenberg, *J. Org. Chem.*, 1971, **36**, 797.
2 T. J. Katz, L. Liu, N. D. Willmore, J. M. Fox, A. L. Rheingold, S. Shi, C. Nuckolls and B. H. Rickman, *J. Am. Chem. Soc.*, 1997, **119**, 10054.
3 K. Paruch, L. Vyklicky, T. J. Katz, C. D. Incarvito and A. L. Rheingold, *J. Org. Chem.*, 2000, **65**, 8774.
4 K. Paruch, T. J. Katz, C. Incarvito, K. C. Lam, B. Rhatigan and A. L. Rheingold, *J. Org. Chem.*, 2000, **65**, 7602.
5 S. D. Dreher, D. J. Weix and T. J. Katz, *J. Org. Chem.*, 1999, **64**, 3671.
6 M. Miyasaka, A. Rajca, M. Pink and S. Rajca, *J. Am. Chem. Soc.*, 2005, **127**, 13806.
7 A. Rajca, M. Miyasaka, M. Pink, H. Wang and S. Rajca, *J. Am. Chem. Soc.*, 2004, **126**, 15211.
8 M. Miyasaka and A. Rajca, *Synlett*, 2004, 177.
9 C. Nuckolls, T. J. Katz, G. Katz, P. J. Collings and L. Castellanos, *J. Am. Chem. Soc.*, 1999, **121**, 79.
10 M. J. Marsella, *Acc. Chem. Res.*, 2002, **35**, 944.
11 J. P. Collin, C. Dietrich-Buchecker, P. Gavina, M. C. Jimenez-Molero and J. P. Sauvage, *Acc. Chem. Res.*, 2001, **V34**, 477.
12 Y. Liu, A. H. Flood, P. A. Bonvallett, S. A. Vignon, B. H. Northrop, H. R. Tseng, J. O. Jeppesen, T. J. Huang, B. Brough, M. Baller, S. Magonov, S. D. Solares, W. A. Goddard, C. M. Ho and J. F. Stoddart, *J. Am. Chem. Soc.*, 2005, **127**, 9745.
13 P. Rempala and B. T. King, *J. Chem. Theory Comput.*, 2006, **2**, 1112.
14 J. Roncali, *Chem. Rev.*, 1997, **97**, 173.
15 J. Roncali, *Chem. Rev.*, 1992, **92**, 711.
16 *Handbook of conducting polymers*, ed. T. J. Skotheim, Dekker, New York, 1986.
17 *Handbook of Conducting Polymers*, ed. T. A. Skotheim, R. L. Elsenbaumer and J. R. Reynolds, Marcel Dekker, Inc., New York, 2nd edn, 1998.
18 M. G. Reinecke and J. G. Newsom, *J. Am. Chem. Soc.*, 1976, **98**, 3021.
19 M. J. Marsella and R. J. Reid, *Macromolecules*, 1999, **32**, 5982.
20 M. J. Marsella, R. J. Reid and L. S. Wang, *Abstr. Pap. Am. Chem. Soc.*, 2001, **222**, 283–PMSE.
21 M. J. Marsella, K. Yoon and F. S. Tham, *Org. Lett.*, 2001, **3**, 2129.
22 M. J. Marsella, R. J. Reid, S. Estassi and L. S. Wang, *J. Am. Chem. Soc.*, 2002, **124**, 12507.
23 M. J. Marsella, K. Yoon, A. Almutairi, S. K. Butt and F. S. Tham, *J. Am. Chem. Soc.*, 2003, **125**, 13928.
24 A. Almutairi, F. S. Tham and M. J. Marsella, *Tetrahedron*, 2004, **60**, 7187.
25 A. Almutairi, K. Yoon, F. Tham and M. J. Marsella, *Pure Appl. Chem.*, 2006, **78**, 777.
26 R. D. McCullough, R. D. Lowe, M. Jayaraman and D. L. Anderson, *J. Org. Chem.*, 1993, **58**, 904.
27 R. D. McCullough, S. Tristram-Nagel, S. P. Williams, R. D. Lowe and M. Jayaraman, *J. Am. Chem. Soc.*, 1993, **115**, 4910.
28 R. D. McCullough, *Adv. Mater.*, 1998, **10**, 93.
29 K. Tamao, S. Kodama, I. Nakajima and M. Kumada, *Tetrahedron*, 1982, **38**, 3347.
30 T. Saika, M. Irie and T. J. Shimidzu, *J. Chem. Soc., Chem. Commun.*, 1994, 2123.
31 M. Irie, *Chem. Rev.*, 2000, **100**, 1683.
32 M. Irie, *Chem. Rev.*, 2000, **100**, 1685.
33 H. E. Katz, L. Torsi and A. Dodabalapur, *Chem. Mater.*, 1995, **7**, 2235.
34 M. J. Marsella and R. J. Reid, *Macromolecules*, 1999, **V32**, 5982.
35 A. E. Reed and F. Weinhold, *J. Chem. Phys.*, 1985, **83**, 1736.
36 A. E. Reed, R. B. Weinstock and F. Weinhold, *J. Chem. Phys.*, 1985, **83**, 735.
37 A. E. Reed, F. Weinhold, L. A. Curtiss and D. J. Pochatko, *J. Chem. Phys.*, 1986, **84**, 5687.
38 E. D. Glendening, J. K. Badenhoop and F. Weinhold, *J. Comput. Chem.*, 1998, **19**, 628.

39 E. D. Glendening and F. Weinhold, *J. Comput. Chem.*, 1998, **19**, 593.
40 E. D. Glendening and F. Weinhold, *J. Comput. Chem.*, 1998, **19**, 610.
41 L. Venkataraman, J. E. Klare, I. W. Tam, C. Nuckolls, M. S. Hybertsen and M. L. Steigerwald, *Nano Lett.*, 2006, **6**, 458.
42 M. J. Marsella, R. J. Newland, P. J. Carroll and T. M. Swager, *J. Am. Chem. Soc.*, 1995, **117**, 9842.
43 M. J. Marsella, P. J. Carroll and T. M. Swager, *J. Am. Chem. Soc.*, 1995, **117**, 9832–9841.
44 T. R. Kelly, J. P. Sestelo and I. Tellitu, *J. Org. Chem.*, 1998, **63**, 3655.
45 T. R. Kelly, I. Tellitu and J. P. Sestelo, *Angew. Chem., Int. Ed. Engl.*, 1997, **36**, 1866.
46 T. R. Kelly, H. De Silva and R. A. Silva, *Nature*, 1999, **401**, 150.
47 G. S. Kottas, L. I. Clarke, D. Horinek and J. Michl, *Chem. Rev.*, 2005, **105**, 1281.
48 T. C. Bedard and J. S. Moore, *J. Am. Chem. Soc.*, 1995, **117**, 10662.
49 M. A. Garcia-Garibay, *Proc. Natl. Acad. Sci. U. S. A.*, 2005, **102**, 10771.
50 H. H. Jian and J. M. Tour, *J. Org. Chem.*, 2003, **68**, 5091.
51 T. Shima, F. Hampel and J. A. Gladysz, *Angew. Chem., Int. Ed.*, 2004, **43**, 5537.
52 J. K. Gimzewski, C. Joachim, R. R. Schlittler, V. Langlais, H. Tang and I. Johannsen, *Science*, 1998, **281**, 531.
53 R. A. van Delden, M. K. J. ter Wiel, M. M. Pollard, J. Vicario, N. Koumura and B. L. Feringa, *Nature*, 2005, **437**, 1337.
54 H. Iwamura and K. Mislow, *Acc. Chem. Res.*, 1988, **21**, 175.
55 J. J. Hopfield, J. N. Onuchic and D. N. Beratan, *Science*, 1988, **241**, 817.

